Are Halos of Collisionless Cold Dark Matter Collisionless?

Chung-Pei Ma and Michael Boylan-Kolchin
Departments of Astronomy and Physics, University of California at Berkeley, Berkeley, CA 94720

Much recent discussion about dark matter has been centered on two seemingly independent problems: the abundance of substructure in dark matter halos, and the cuspiness of the halos' inner density profile. We explore possible connections between the two problems by studying the gravitational scattering effects due to subhalos on the phase-space distribution of dark matter particles in the main halos. Our series of controlled numerical experiments indicates that the number and mass density of subhalos can be high enough to cause the collisionless dark matter particles in the inner part of a main halo to diffuse, flattening the main halo's inner cusp within a few dynamical times. Depending on the masses and concentration of the subhalos, the inner density profile of the whole system (main plus sub halos) can either steepen or flatten. Subhalo accretion can therefore introduce significant scatter in the inner density profiles of dark matter halos, offering a possible explanation for the range of profiles seen in both observations and cosmological simulations.

Particles undergo random walks and diffusion through collisional scatterings. The most noted example is the Brownian motion of small macroscopic particles, whose velocities exhibit frequent sudden changes due to impulsive collisions with individual molecules in a liquid. On astrophysical scales, stars also undergo random walks in velocity space due to gravitational scatterings with, e.g., other stars or giant interstellar clouds in a galaxy [1].

Recent high resolution N-body simulations of hierarchical structure formation in cold dark matter (CDM) models have shown that spatial distribution of dark matter in galaxy-hosting halos is not entirely smooth. Instead, roughly 10% of a halo's mass is in the form of hundreds to thousands of smaller, dense satellite subhalos of varying mass [2]. In this Letter we examine whether these subhalos can be the source of a fluctuating gravitational potential that produces collisional transport of CDM particles in the main halo, even when the self-interaction of CDM is *collisionless*. Our approach is based on numerical simulations and addresses the fully nonlinear regime of halo-subhalo interaction; a complementary approach is pursued by [3], who have used second-order cosmological perturbation theory to derive a kinetic equation for the phase-space distribution of halo dark matter particles.

Physics of Diffusion.—A test particle of mass M_t and velocity $\vec{v}_t$ experiences dynamical friction and exhibits random walks (in velocity space) as it moves through the gravitational potential of background particles of mass M_b. Both processes change the test particle velocity ($\Delta v_i, i = 1, 2, 3$) and energy (ΔE): the dynamical friction is described by the diffusion coefficient $D(\Delta v_\parallel)$ where $d\vec{v}_t/dt = \hat{v}_t D(\Delta v_\parallel)$; the random walk is described by the diffusion tensor $D(\Delta v_i \Delta v_j)$. The rate of change of the kinetic energy of the test particle is $D(\Delta E) = M_t \Sigma_i [v_i\, D(\Delta v_i) + \frac{1}{2} D(\Delta v_i^2)]$ [4]. For background particles with a uniform mass density ρ_b and an isotropic Maxwellian velocity distribution with dispersion σ_b, it is

$$D(\Delta E) = 4\pi G^2 \frac{\rho_b M_t}{v_t} \ln\Lambda \left\{ -M_t F(x) + M_b [\mathrm{erf}(x) - F(x)] \right\}, \quad (1)$$

where $\ln\Lambda$ is the Coulomb logarithm, $x = v_t/\sqrt{2}\sigma_b$, and $F(x) = \mathrm{erf}(x) - 2x\, \exp(-x^2)/\sqrt{\pi}$. Note that this equation is valid for arbitrary ratios of M_t/M_b [5]. The first term in Eq. (1) describes the energy *loss* of the test particle due to dynamical friction. In the standard Chandrasekhar picture, a large test mass M_t scatters off a sea of small background particles with mass M_b. In this limit ($M_t \gg M_b$), the first term in Eq. (1) (due to the test particle polarizing the background medium) dominates, and the second term is typically ignored.

Our focus in this Letter is different. We are interested in the effects on the dark matter particles in the main halo (our test particles) due to the ensemble of subhalos (our background particles). The relevant mass range, $M_t \ll M_b$, is therefore opposite of that in the last paragraph. The polarization cloud term is completely negligible. Instead, the key process is the second term in Eq. (1), which describes the *heating* of the test particle due to stochastic fluctuations in the background particles. Changes in the potential due to the distribution of dark matter substructure are the dominant scattering source in our study.

Effects of Diffusion.—We perform a series of fully dynamical simulations using `GADGET`, a publicly available N-body tree code [6], to follow the evolution of dark matter in a parent halo containing an ensemble of subhalos. To study the dynamical interplay between a main halo and its subhalos in a controlled and semi-realistic way, we use subhalo properties similar to those from earlier full-scale cosmological simulations [2]. This strategy allows us to perform a suite of numerical experiments to quantify the effects due to a wider range of subhalo masses, concentration, and orbits than is possible with large cosmological simulations.

Initially the particles in the main halo are given an NFW radial density profile [7]: $\rho(r) = \rho_{crit}\bar{\delta}/[x(1+x)^2]$, where $x = r/r_s$, $\bar{\delta} = 200c^3/3[\ln(1+c) - c/(1+c)]$, and the concentration parameter $c = r_{vir}/r_s$ is the ratio of the halo's virial to scale radius. We use a total of 10^6 simulation particles for the main halo and a force soften-

ing of $0.015r_s$. The particle velocities are drawn from a local isotropic Maxwellian distribution where the radius-dependent velocity dispersion is computed from the Jeans equation (see [8] for details and tests of a similar set-up). This velocity setup may cause an NFW halo's inner cusp to artificially flatten initially [9]. To work around this problem, we evolve an NFW halo in isolation for $\sim 8\,t_{dyn}$ (where $t_{dyn}^2 \equiv 3\pi/16G\rho(r_s)$) and use this evolved halo as our initial main halo. Our tests have shown that this halo, which does differ slightly at $r \leq 0.1r_s$ from its original NFW structure, is extremely stable over the next $10t_{dyn}$ at all scales $r \geq 0.03r_s$.

To simulate the effects of substructures on dark matter halos, we add ~ 1000 subhalos to the main halo. The subhalo masses are drawn from $dn_{sub}/dM_{sub} \propto M_{sub}^{-1.7}$, similar to those found in cosmological simulations [2]. Initially the subhalos are placed within the virial radius of the main halo either with a top-hat or r^{-2} radial number density distribution (see Fig. 1 for a comparison). The center-of-mass velocities of the subhalos are drawn from a local isotropic distribution identical to that of the CDM particles in the main halo. Simulations indicate that both CDM particles and subhalos are likely to develop mild velocity anisotropies in the outer part of the main halo [10] but this effect should be small.

Point-Mass Subhalos.—In the simplest case, we represent each subhalo as a point mass. This model is unrealistic and overestimates the relaxation effect since it ignores mass losses due to tidal stripping. However, it serves as a test case for the validity of the standard Chandrasekhar formula (see Eq. [2]) and approximates the effects of dense baryonic clumps that can survive into halo centers.

Fig. 1 shows the results of our point-mass subhalo simulations in dimensionless units, which hold for halos of different masses at appropriately scaled cosmic times (see caption). It illustrates that point-mass subhalos can indeed result in significant flattening in the inner ρ of a main halo within a few (inner) dynamical times. The amount of flattening is sensitive to the masses of the several most massive subhalos present in the main halo since these subhalos dominate the energy exchange with the dark matter in the main halo, as seen in Eq. (1). We have performed two identical runs – one having 999 point subhalos (dashed curves); the other having 996 point subhalos (dotted) without the top 3 most massive subhalos in the 999 run – to test the effect of massive subhalos. The subhalos are placed initially within the main halo with r^{-2} distribution. Fig. 1 shows the heating of the main halo in the 996 run occurs at a later time (between 2.8 and $6.9\,t_{dyn}$) and also leads to less flattening than the 999 run. The total subhalo mass in the 999 and 996 runs is 7.02% and $3.29\%M_{main}$; the three most massive subhalos in the 999 run have masses 1.51%, 1.25%, and $0.97\%M_{main}$.

The two 999 subhalos runs in Fig. 1 illustrate the dependence of the relaxation timescales on the subhalo spatial distribution. In accordance with Eq. (1), the inner part of the main halo flattens more quickly for the r^{-2} case than the top-hat case. For the latter, the initial main halo $\rho(r)$ is unchanged through $6.9\,t_{dyn}$ and then flattens quickly in three t_{dyn}. The stabilized main halo profile (at $9.7\,t_{dyn}$; bottom dot-dashed) is similar to the other 999 case, so the difference due to different subhalo spatial distributions is mainly in the timescales.

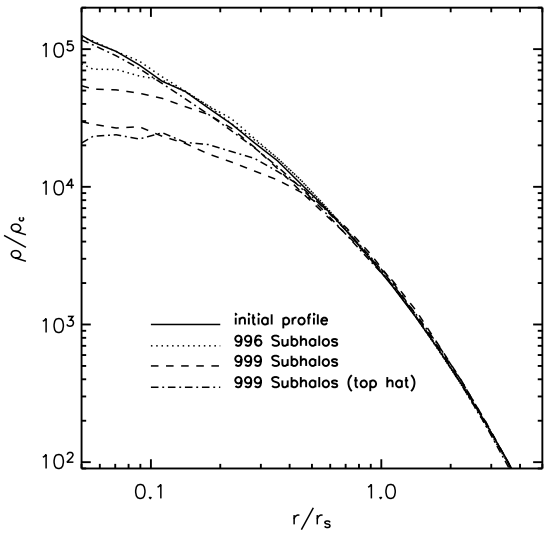

FIG. 1: Evolution of the radial density profile of a main halo (with $c_{main} = 5.2$) containing 996 vs. 999 point-mass subhalos. The dotted (996) and dashed (999) curves are for identical simulations except for the removal of the three most massive subhalos. The inner $\rho(r)$ decreases with time from $t = 0$ (solid) to $2.8\,t_{dyn}(r_s)$ (upper of each pair) and $6.9\,t_{dyn}(r_s)$ (lower of each pair); $t_{dyn}(r_s)$ is 0.072, 0.25, and 0.45 h^{-1} Gyr for a $10^8 M_\odot$ (at $z = 4$), $10^{12} M_\odot$ ($z = 1$), and $10^{14} M_\odot$ ($z = 0$) main halo. The dot-dashed curves compare the same 999 run as the dashed curves except the subhalo centers are placed initially with a tophat instead of r^{-2} distribution; the main halo here flattens later between $6.9\,t_{dyn}$ (upper dot-dashed) and $9.7\,t_{dyn}$ (lower). Without the subhalos, we have tested that the solid curve does not change over at least $10\,t_{dyn}$.

Puffy Subhalos.—To model the subhalos more realistically, we perform a series of simulations in which the 10 most massive subhalos are given NFW profiles, while 989 lower mass subhalos (all $< 0.1\%\ M_{main}$) are represented by point particles since they would suffer little mass loss. The total mass in subhalos in these cases is equal to either 7.02 or $10.3\%M_{main}$, where the ten most massive subhalos comprise 5.2% or 9.0%. The 7.02% model has the same subhalo mass spectrum as in the point-mass runs above, while the 10.3% model uses a different realization in which the three most massive subhalos are 4.66, 2.09, and $1.00\%M_{main}$.

Fig. 2 shows $\rho(r)$ from our simulations of NFW subha-

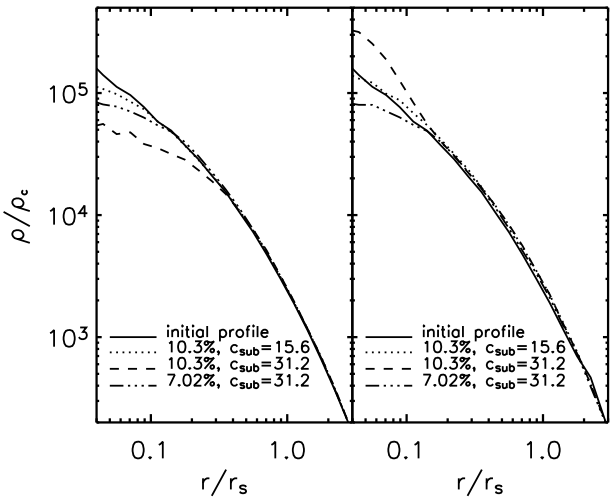

FIG. 2: Radial density profile of a main halo (with $c_{main} = 5.2$) containing puffy subhalos. The panels compare $\rho(r)$ of the main halo (left) vs main-plus-subhalos (right) initially (solid) and after $5.55\,t_{dyn}$ of evolution (other 3 curves). Three simulations with different subhalo concentration ($c_{sub} = 15.6$ vs 31.2) and total subhalo masses (10.3% vs 7% of main halo mass) are shown.

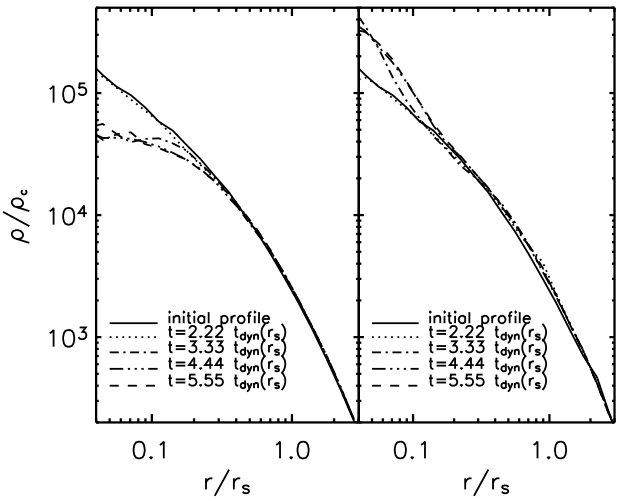

FIG. 3: Time evolution of ρ of the main halo (left) and main-plus-subhalo (right) for the $c_{sub} = 31.2$, 10.3% subhalo run in Fig. 2. Most of the evolution occurs between 2.22 and $3.33\,t_{dyn}$.

los with three combinations of subhalo concentration c_{sub} and subhalo mass fraction. Since the subhalos can now shed mass in complicated ways, we compute $\rho(r)$ both from the main halo particles only (left) and from all particles (right). Flattening in the main halo $\rho(r)$ is seen for all three cases. The amount of flattening is more severe when a higher mass fraction of the system is in subhalos, and when the subhalos have a higher c_{sub} because more centrally concentrated subhalos suffer less tidal mass loss as they sink towards the main halo center.

The inner cusp of the *total* mass, however, can steepen, remain the same, or flatten, depending on the competition between the addition from subhalo masses deposited in the central regions and the removal of main halo particles due to gravitational heating. The three models in Fig. 2 (right panel) showcase the three outcomes. The subhalos in the 7.02% model are not massive enough to add much mass, so both the main and total $\rho(r)$ are flattened ($\sim r^{-0.75}$) in $\sim 6\,t_{dyn}$. In contrast, in the model with 10.3% subhalo mass and $c_{sub} = 31.2$, the mass added by the most massive subhalos (the top two have 4.66% and 2.09% M_{main}) more than compensate for the flattening in the main halo, leading to a steeper than r^{-1} inner cusp. Fig. 3 illustrates this model in more detail with five time outputs: most of the evolution occurs within one dynamical time after $2.2\,t_{dyn}$ when tje most massive subhalos make their way to the center. [11] showed that accreting one massive concentrated subhalo of $10\%M_{main}$ can also produce a cusp in an initially cored halo.

We emphasize that the inner $\rho(r)$ of a halo depends sensitively on the location of the halo center used to compute $\rho(r)$. Although the initial momenta of the subhalos are drawn from an isotropic distribution, fluctuations typically introduce a small center-of-mass (COM) motion for the entire system: a COM velocity $\sim 2\%$ of the main halo circular velocity was not uncommon, resulting in COM offsets of $\sim r_s$ in $\sim 10\,t_{dyn}$. Neglecting this effect and naïvely using a halo's initial center as the center for subsequent outputs would lead to a flattened $\rho(r)$. We use a more physical halo center (e.g. iteratively determined COM, most bound particle, or COM of the 500 most bound particles; all three give nearly identical results), which eliminates this spurious flattening.

Timescale.—How do the timescales seen in the simulations compare with the simple energy exchange time predicted by Eq. (1)? The latter predicts

$$t_{relax} = \frac{\frac{1}{2}M_t v_t^2}{|D(\Delta E)|} \approx \frac{1}{8\pi G^2 \ln\Lambda}\frac{v_t^3}{\rho_b M_b}\frac{\sqrt{\pi}}{2xe^{-x^2}}\,, \qquad (2)$$

where the second equality assumes $M_t \ll M_b$. In our study, this gives the timescale for heating the dark matter particles from a background of subhalos of mass M_{sub}, density ρ_{sub} in the main halo, and COM velocity dispersion σ_{sub}. Re-expressing it in terms of the main halo's virial mass M_{main} and radius r_v, and 1-d velocity dispersion at r_v, $\sigma(r_v)$, we obtain

$$t_{relax} \approx \frac{0.12}{H(z)}\frac{10}{\ln\Lambda}\frac{\rho_{crit}M_{main}}{\rho_{sub}M_{sub}}\left(\frac{v_t}{\sigma(r_v)}\right)^3\frac{\sqrt{\pi}}{2xe^{-x^2}}\,, \quad (3)$$

where the Hubble time at redshift z is $H^{-1}(z) = 9.78\,\mathrm{Gyr}\,h^{-1}[\Omega_m(1+z)^3+\Omega_\Lambda]^{-1/2}$. Let $dn_{sub}/dM_{sub} \propto$

$M_{sub}^{-\alpha}$ be the subhalo mass function (assuming $\alpha > 1$), β be the ratio of the total mass in subhalos to M_{main}, and γ be the ratio of the most massive subhalo to M_{main}. We find $\rho_{crit} M_{main}/\rho_{sub} M_{sub} = (3-\alpha)/(2-\alpha)/(200\beta\gamma)$; for the 999 point-mass model shown in Fig. 1, this ratio is about 19. The local dynamical time at the scale and virial radius of an NFW halo with $c_{main} = 5.2$ is $t_{dyn}(r_s) = 0.14\, t_{dyn}(r_v) = 0.046\, H^{-1}(z)$ (assuming unity for factors involving velocities, which is likely an underestimate), so we find $t_{relax} \sim 2.3\, H^{-1}(z) \sim 50\, t_{dyn}(r_s) \sim 7\, t_{dyn}(r_v)$. This is at least 5 times longer than the flattening timescale seen in the 999 point-mass top-hat simulation in Fig. 1. Eqs. (1)-(3), however, are valid only for a stationary, infinite, homogeneous background with a global Maxwellian velocity distribution [5]. In our study, the background is an ensemble of dark matter subhalos, themselves moving in a deeper main halo potential and experiencing dynamical friction and tidal mass losses. While Eqs. (1)-(3) elucidate the energy exchange between subhalos and dark matter particles, it is not surprising that they do not predict the exact timescales seen in simulations.

We have performed a test run with 1000 point-mass subhalos of equal mass where the total subhalo mass is 15% M_{main}. This subhalo mass spectrum is unrealistic, but this run provides an additional test case and a comparison case for a recent cluster galaxy study [12]. Since each subhalo mass in our test run is only 0.015% $M_{\rm main}$, ~ 100 times smaller than the most massive subhalos in Fig. 1, t_{relax} in Eq. (3) increases by a factor of ~ 100, too long to result in change in the inner halo profile. We indeed did not see any flattening over $\sim 9\, t_{dyn}$ (at r_s) in our simulation.

Implications.—Our series of controlled numerical experiments indicates that collisionless dark matter particles in the inner parts of galaxy and cluster halos can gain energy through gravitational scatterings off concentrated dark matter subhalos, altering the inner density cusp of the main halo within a few dynamical times. These subhalos appear ubiquitous in high resolution cosmological simulations and provide the source of fluctuations for the diffusion described by Eq. (1). We have studied the evolution of halos under the influence of only one generation of subhalos, while real halos grow continuously by accretion and mergers. The effects we have seen, however, suggest that fluctuations due to subhalos in parent halos are important for understanding the time evolution of dark matter density profiles and the halo-to-halo scatter of the inner cusp seen in recent ultra-high resolution cosmological simulations [13]. We have shown that this scatter may be explained by subhalo accretion histories: when we allow for a population of subhalos of varying concentration and mass, the total inner profile of dark matter can either steepen or flatten.

Recent observations of dwarf galaxy rotation curves based on CO and Hα emission find significant variations in the inner profile, ranging from a core to $\sim r^{-1}$ [14]. While baryonic physics can influence the central mass profile, the purely gravitational physics of subhalo scattering studied here may also accommodate the variations seen in these observations. Conversely, maintaining a stable and universal inner profile would require a "quiescent" accretion history not involving concentrated massive subhalos. Halos in cosmological models with truncated small-scale power (e.g. warm dark matter) contain many fewer satellites [15]; their inner cusps should therefore be less prone to variations due to subhalo accretion.

We thank J. Arons, E. Bertschinger, A. Dekel, N. Gnedin and A. Kravtsov for useful discussions. The simulations were performed at NERSC. C.-P. M is partially supported by a Cottrell Scholars Award from the Research Corporation and NASA grant NAG5-12173.

[1] S. Chandrasekhar, Rev. Mod. Phys. **15**, 1 (1943); L. Spitzer & M. Schwarzschild, ApJ **114**, 385 (1951).
[2] A. Klypin et al. ApJ **522**, 82 (1999); S. Ghigna et al. ApJ **544**, 616 (2000); B. Moore et al. PRD **64**, 063508 (2001); A. Kravtsov, O. Gnedin & A. Klypin, astro-ph/0401088; G. De Lucia et al. MNRAS **348**, 333 (2004).
[3] C.-P. Ma and E. Bertschinger, ApJ, in press (2004).
[4] J. Binney and S. Tremaine, *Galactic Dynamics*, p513 (Princeton U. Press, Princeton, 1987).
[5] R. Nelson & S. Tremaine, MNRAS **306**, 1 (1999); J. Bekenstein & E. Maoz, ApJ **390**, 79 (1992).
[6] V. Springel, N. Yoshida & S.D.M. White, New Astron **6**, 79 (2001).
[7] J. Navarro, C. Frenk & S.D.M. White, ApJ **490**, 493 (1997).
[8] M. Boylan-Kolchin & C.-P. Ma, MNRAS **349**, 1117 (2004).
[9] S. Kazantzidis, J. Magorrian, & B. Moore, ApJ **601**, 37 (2004); Tasitsiomi et al. astro-ph/0311062.
[10] J. Diemand, B. Moore & J. Stadel, astro-ph/0402160
[11] A. Dekel et al. ApJ **588**, 680 (2003).
[12] A. El-Zant et al., astro-ph/0309412.
[13] J. Navarro et al., astro-ph/0311231; D. Reed et al., astro-ph/0312544; J. Diemand, B. Moore & J. Stadel, astro-ph/0402267.
[14] e.g. A. Bolatto et al. astroph/0311259; A. Borriello & P. Salucci MNRAS **323**,285 (2001).
[15] P. Bode, J. Ostriker & N. Turok, ApJ **556**, 93 (2001); P. Colin, V. Avila-Reese & O. Valenzuela, ApJ **542**, 622 (2000)